Journal of Pharmacokinetics and Pharmacodynamics (2019) 46:513–529
https://doi.org/10.1007/s10928-019-09648-1

ORIGINAL PAPER

Computational framework for predictive PBPK-PD-Tox simulations of opioids and antidotes

Carrie German[1] · Minu Pilvankar[2] · Andrzej Przekwas[1]

Received: 13 February 2019 / Accepted: 29 July 2019 / Published online: 8 August 2019

Abstract

The primary goal of this work was to develop a computational tool to enable personalized prediction of pharmacological disposition and associated responses for opioids and antidotes. Here we present a computational framework for physiologically-based pharmacokinetic (PBPK) modeling of an opioid (morphine) and an antidote (naloxone). At present, the model is solely personalized according to an individual's mass. These PK models are integrated with a minimal pharmacodynamic model of respiratory depression induction (associated with opioid administration) and reversal (associated with antidote administration). The model was developed and validated on human data for IV administration of morphine and naloxone. The model can be further extended to consider different routes of administration, as well as to study different combinations of opioid receptor agonists and antagonists. This work provides the framework for a tool that could be used in model-based management of pain, pharmacological treatment of opioid addiction, appropriate use of antidotes for opioid overdose and evaluation of abuse deterrent formulations.

Keywords Opioids · PBPK · Modeling · Pharmacodynamics · Naloxone

Introduction

Over the past two decades in the United States, there has been a dramatic rise in prescription pain medications and in misuse of opioids. Pain medications are currently the most widely prescribed class of drugs in the US, with an estimated 245 million prescriptions dispensed in 2014 [1, 2]. At present prescription opioids are an important component of chronic pain management. However, abuse and misuse of these frequently prescribed products (25 million per year) have created a national epidemic of addiction, overdose, and death [3]. In 2015, 12.5 million people (4.7% of the population) in the USA older than 12 years of age reported misusing prescription opioids and over 2 million people meet the criteria for severe opioid use disorder (OUD) [4, 5].

Effective pharmacologic management of both acute and chronic pain requires finding an appropriate balance between analgesic effects and associated side effects. Unfortunately, the patient pharmacological responses to pain medications are highly variable, ranging from desirable pain relief, to inadequate pain control, to reward and pleasure feeling, to the development of medication withdrawal symptoms, opioid tolerance and addiction. The pharmacological response greatly depends on the opioid used (type, route of administration, dose, formulation, addiction status), individual anatomy (age, gender, body weight), genetic factors regulating opioid pharmacokinetics (metabolism, transporters) and pharmacodynamics (binding to neuronal receptors and signal transduction). This variability makes it also difficult to prescribe pain medication for a specific patient with a specific and subjective level of pain. Owing to various opioids having different speeds and durations of action, selection of an adequate antidote dose is challenging. Personalized mathematical models of opioid pharmacokinetics (PK) and pharmacodynamics (PD) can become valuable tools in model-based management of pain, pharmacological treatment of opioid

Electronic supplementary material The online version of this article (https://doi.org/10.1007/s10928-019-09648-1) contains supplementary material, which is available to authorized users.

✉ Carrie German
carrie.german@cfdrc.com

[1] CFD Research Corp., Huntsville, AL 35806, USA

[2] School of Chemical Engineering, Oklahoma State University, Stillwater, OK 74078, USA

addiction and safer use of antidotes for opioid overdose [6–11].

This paper presents a computational framework for modeling opioid PK, PD and neurophysiological responses. Here we describe the physiology-based pharmacokinetics (PBPK) model for an opioid (morphine) and an antidote (naloxone) as well as a minimal PD model in the form of morphine induction and naloxone reversal of respiratory depression. The PBPK model has been validated on human clinical data and was used to conduct parametric simulations of the naloxone rescue effects as a function of time delay and route of naloxone administration (IV) after morphine intoxication. The model is being extended to naloxone nasal administration.

Methods

A simulation framework for opioid PK, PD and neuroadaptation

Recent progress in mechanistic, physiology and neurobiology-based mathematical models of opioid pharmacology provides the foundation for the development of personalized and population-based computational models of opioid pharmacology and neuroadaptation [7, 9, 12, 13]. The ultimate use of such a framework would be to predict individual-specific analgesic effects (dose–response) for various types of opioids, addiction prevention medications and overdose reversal treatments. Such framework should comprise several components representing (i) opioid chemical and pharmacological properties, (ii) individual-specific anatomy, physiology and genetic characteristics, (iii) mechanistic models of whole-body PK and (iv) tissue/cellular PD effects. Figure 1 schematically represents various components of such a simulation framework.

As the majority of opioid action takes place in the central nervous system (CNS), such framework should also include brain region specific drug/metabolite biodistribution, receptor binding kinetics, neurotransmission and neurobiology-based models of tolerance and addiction [14–17].

Ultimately such a modeling framework should be deployed on the cloud, accessible to mobile devices and capable of collecting signals from wearable physiological sensors to enable prediction of an impending overdose, and automatically administer medical countermeasures [2]. The present opioid PBPK and PD simulation tools have been deployed on cloud computing servers and are freely accessible for web-based simulations (http://medicalavatars.cfdrc.com/index.php/opioids/).

Population-based models of morphine and naloxone pharmacokinetics

PK models describe the relationship between drug concentration(s) in the body as a function of time. Conventional PK models divide the body into relatively few compartments (central, peripheral) and solve simple ordinary differential equations (ODEs) for drug concentration in these compartments using lumped kinetic constants [18]. More advanced models of physiology-based PK (PBPK) represent the human body as a network of individual organs supplied by the artery and drained by the venous pool [19].

PBPK models are expressed as a system of one-dimensional (1D) ODEs which govern drug mass transport (convection, diffusion and chemical reaction) and characterize the absorption, distribution, metabolism, and elimination of a chemical within the physiologically arranged tissue compartments (e.g., gut, liver, kidney, lungs, brain). PBPK models directly account for body anthropometric and physiological characteristics (body weight, cardiac output, organ blood flow rates, organ blood-tissue surface area, and others). Various representations of individual organs have been used ranging from well-stirred models to organ models with spatially resolved blood and tissue regions [20].

Physiologically-based layout of organ compartments and associated PBPK parameters

In this work we employ a human PBPK model which includes adipose, bone marrow, kidney, liver, spleen, intestine, muscle, brain and lung tissues. The organs and blood are represented as well-stirred compartments. The lung compartment is used as a return from venous to arterial pool (Fig. 2) through which all blood eventually passes to become oxygenated, and as such is assumed to have a blood flow rate equal to the total cardiac output. The liver and connected organs (spleen and intestine) are included to account for hepatic metabolism and circulation.

The residual compartment accounts for the volume and flow of all organs and tissues not specifically depicted/characterized in the model. The residual compartment is divided into blood and tissue subcompartments to represent vascularization differences (poorly and highly perfused). As assumed in a previous study [21], our model assumes blood comprises 5% of the total residual volume with the remainder being tissue. Selected organ volumes, blood flow rates, weight fractions and densities for humans obtained from literature are shown in Table 1. The residual blood volumetric flow rate was calculated by subtracting the selected organ blood flow rates from the total blood flow rate. The total residual mass was calculated similarly.

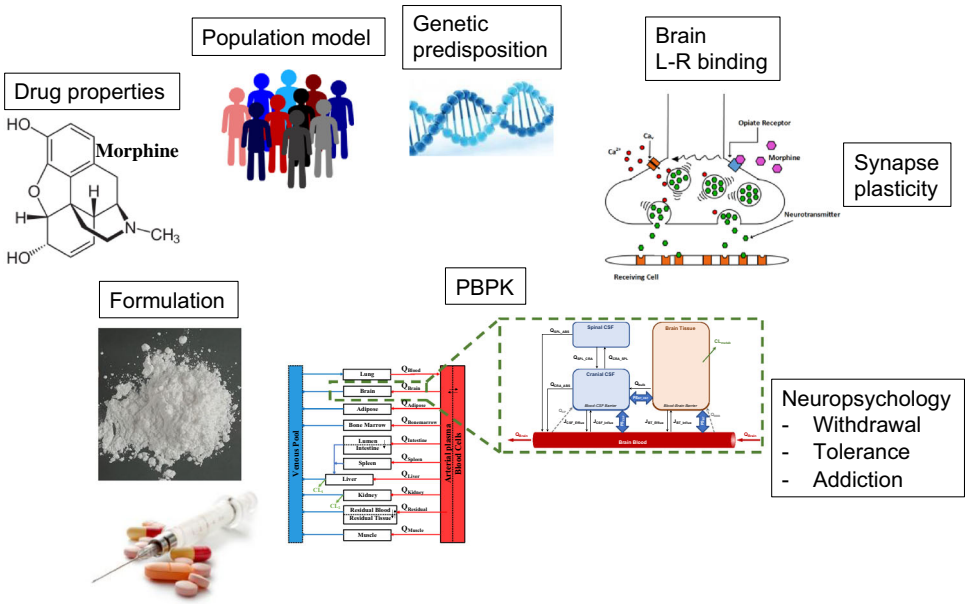

Fig. 1 Main components of the computational framework for predictive PBPK-PD-Tox simulations of opioids and antidotes

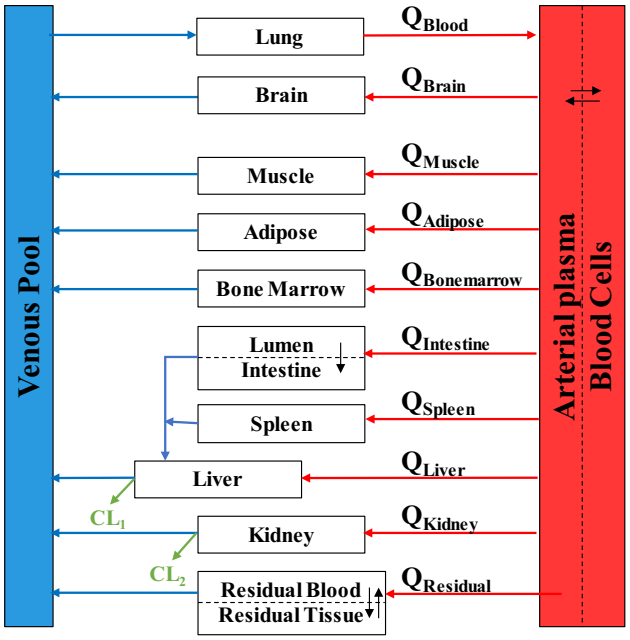

Fig. 2 PBPK general layout of organ and blood compartments

All organ compartment and subcompartment volumes depend on the total mass and are scaled for experiments where the average human mass is anything other than 70 kg. Note that the liver exit flow rate is equal to the sum of the spleen, intestine and liver inlet flow rates.

With the brain compartment housing the primary opioid receptor targets, a higher resolution model was needed. The advanced brain model used in our simulation is adapted from [22]. The μ-opioid receptor is a transmembrane receptor that is activated by opioid compounds in the brain interstitial fluid, and as such requires further resolution of the brain tissue compartment described in literature [22]. Thus, in our model, the brain tissue compartment is divided into 5 sub-compartments: brain tissue, brain blood, brain interstitial fluid (ISF), cranial cerebrospinal fluid (CSF) and spinal CSF (Fig. 3). Brain sub-compartment volumes used in simulation are shown in Table 2.

A number of transport phenomena are captured in the model, including: fluid flow (Q_i), active transport ($J_{i\_efflux/influx}$) and passive permeability (PS_i). Physiological fluid flow values used in simulation and shown in Fig. 3 are provided in Table 2.

Governing equations for drug transport

Organ transport (excluding brain and residual tissues) is assumed to follow perfusion-limited kinetics characterized by,

$$V_i \cdot \frac{dC_i}{dt} = Q_i \cdot \left(C_{ART\_PL} - \frac{C_i}{K_i} \right) \quad (1)$$

where V_i represents the compartmental volume, C_i is the concentration, Q_i is the organ specific blood flow rate, C_{ART_PL} represents the arterial plasma concentration entering the organ and K_i represents the tissue specific partition coefficient. The perfusion limited equation for the lungs differs due to the direction of flow,

$$V_{Lung} \cdot \frac{dC_{Lung}}{dt} = Q_{blood} \cdot \left(C_{VEN} - \frac{C_{Lung}}{K_{Lung}} \right) \quad (2)$$

where Q_{blood} is the total cardiac output and C_{VEN} is the venous concentration being carried into the lungs.The residual compartment contains blood and tissue subcompartments, accounting for blood perfusion variation throughout the tissue

Table 1 Physiological parameters for a 70 kg adult male

Organ	Volume[a] (L)	Blood flow rate[a] (L/min)	Weight[d] fraction	Density[e] (g/cm^3)
Arterial Blood	1.928	5.325	0.049	1.058
Venous Blood	3.855			1.058
Lungs	1.253	5.325	0.0137	1.05
Brain	1.553	0.639	0.02068	1.04
Muscle	32.175	0.905	0.44861	1.04
Adipose	10.725	0.266	0.1307	0.923
Bone	9.300	0.266	0.15940	1.4
Kidney	0.330	1.012	0.00602	1.050
Liver	1.808	0.346	0.03283	1.08
Spleen	0.203	0.1065	0.00291	1.06
Intestine	1.770	0.799	0.01557	1.042
Lumen	2680.9[b]	–	0.0362[f]	1.042[g]
Residual	6121.7[c]	0.985	0.08438	1.02[h]

[A]from [65] unless otherwise indicated

[b]Lumen volume = $\text{Weight\_Fraction}_{\text{Lumen}}$ *Human_weight/$\text{Density}_{\text{Lumen}}$

[c]Residual volume = $\text{Weight\_Fraction}_{\text{Residual}}$*Human_weight/$\text{Density}_{\text{Residual}}$

[d]Calculated from PK-SIM data

[e]Taken from Supplementary material for [66]

[f]Lumen Weight Fraction [21]

[g]Lumen Density is assumed to be same intestine

[h]Residual density is the mean of all other densities

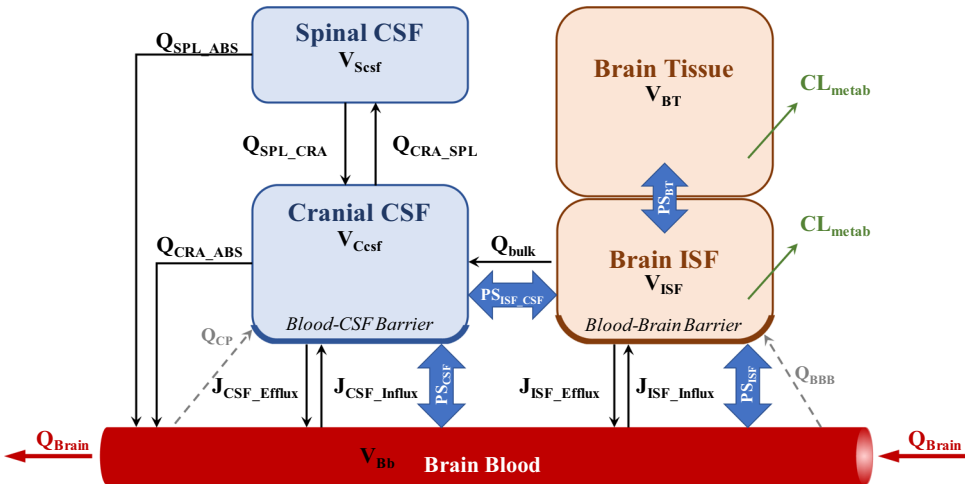

Fig. 3 Sub-compartment layout and transport parameters of the brain model

collective. The rate of change of drug concentration in the residual blood compartment is as follows,

$$V_{RES\_Blood} \cdot \frac{dC_{RES\_Blood}}{dt} = Q_{RES\_Blood} \cdot (C_{ART\_PL} - C_{RES\_Blood}) - PS_{RES\_Blood\_Tissue} \cdot \left(C_{RES\_Blood} - \frac{C_{RES\_Tissue}}{K_{RES\_Tissue}}\right) \quad (3)$$

where $PS_{j\_Blood\_Tissue}$ represents the permeability surface area product for transport from blood to tissue. It was assumed that no partitioning occurred between arterial blood and residual blood, thus the lack of a partition coefficient in the perfusion limited portion of Eq. 3. As such, the ODE for concentration of the residual tissue compartment is characterized by the permeability-limited equation only, given by,

Table 2 Geometric and transport parameters for the resolved brain compartments

Parameter	Value	Reference values
V_{Brain_Blood}	82.1 mL	5% total brain volume [12]
		75 mL [67]
V_{CRA_CSF}	130 mL	[68]
V_{SPL_CSF}	30 mL	[68]
$V_{\_Brain\_Tissue}$	1399 mL	Calculated as residual brain volume
Q_{CP} CSF production	03500 mL/min	0.3–0.4 mL/min [69]
		0.41–0.19 mL/min (age dependent) [70]
Q_{SPL_CRA}	0.1167 mL/min	7 mL/h [71]
Q_{SPL_Abs}	0.1330 mL/min	Calculated 38% of total Q_{CP} [72]
Q_{CRA_Abs}	0.2170 mL/min	Calculated 62% of total Q_{CP} [72]
Q_{bulk}	0.0875 mL/min	25% of total CSF production [72, 73]
Q_{BBB}	0.0875 mL/min	Equal to Q_{bulk} from flow balance
Q_{CRA_SPL}	0.3372 mL/min	Calculated from flow balance
fu_{CSF}	1	(Assumed negligible for both drugs)
A_{BBB}	20 m^2	[74]
A_{CSF_BB}	0.02 m^2	[75]
Morphine brain transport parameters		
PS_{ISF_CSF}	1E−1 L/min	Calibrated
PS_{BT}	1E−1 L/min	Calibrated
J_{ISF_Influx}	1E−2 L/min	Calibrated
J_{ISF_Efflux}	1.6E2 L/min	Calibrated
J_{CSF_Influx}	3E−1 L/min	Calibrated
J_{CSF_Efflux}	1E3 L/min	Calibrated
Naloxone brain transport parameters		
PS_{ISF_CSF}	3E−2 L/min	Calibrated
PS_{BT}	5E−1 L/min	Calibrated
J_{ISF_Influx}	3E1 L/min	Calibrated
J_{ISF_Efflux}	5.4E1 L/min	Calibrated
J_{CSF_Influx}	8.9E1 L/min	Calibrated
J_{CSF_Efflux}	3.5E−1 L/min	Calibrated

$$V_{RES\_Tissue} \cdot \frac{dC_{RES\_Tissue}}{dt} = PS_{RES\_Blood\_Tissue} \cdot \left(C_{RES\_Blood} - \frac{C_{RES\_Tissue}}{K_{RES\_Tissue}} \right) \quad (4)$$

In the brain, a system of differential equations was developed to characterize the subcompartmental rate of change of drug concentration using a flux balance formulation. For the brain interstitial fluid compartment the mass balance yields,

$$\begin{aligned} V_{ISF} \frac{dC_{ISF}}{dt} = {} & (Q_{BBB} \cdot C_{Bb}) - (Q_{bulk} \cdot C_{ISF}) \\ & - (CL_{metab} \cdot fu_{ISF} C_{ISF}) \\ & + \left(J_{ISF\_Influx} \cdot fu_{Bb} C_{Bb}\right) \\ & - \left(J_{ISF\_Efflux} \cdot fu_{ISF} C_{ISF}\right) \\ & + PS_{ISF}(fu_{Bb} C_{Bb} - fu_{ISF} C_{ISF}) \\ & + PS_{ISF\_CSF}\left(C_{Ccsf} fu_{CSF} - fu_{ISF} C_{ISF}\right) \\ & - PS_{BT}\left(fu_{ISF} C_{ISF} - fu_{BT} \cdot \frac{C_{BT}}{k_{brain}}\right) \end{aligned} \quad (5)$$

where subscripts *ISF*, *Ccsf* and *Bb* represent the brain interstitial fluid, cranial CSF and brain blood compartments respectively, *V* is the volume, J_{ISF_Influx} and J_{ISF_Efflux} represent active drug transport across the blood–brain barrier (BBB) into and out of the brain tissue respectively, *C* is drug concentration, *PS* is the permeability surface area product, CL_{metab} is the linear metabolic rate of drug metabolism, and *fu* is the unbound drug fraction. The brain tissue mass balance yields,

$$V_{BT}\frac{dC_{BT}}{dt} = PS_{BT}\left(fu_{ISF}C_{ISF} - fu_{BT}\cdot\frac{C_{BT}}{k_{brain}}\right) - \left(CL_{metab}\cdot C_{BT}\cdot fu_{BT}\right) \quad (6)$$

where k_{brain} is the brain tissue to blood partition coefficient and the subscript BT represents the brain tissue compartment. A mass balance over the spinal CSF compartment yields,

$$K_i = \frac{\left[K_{o:w}\times\left(V_{nl,tissue}+0.3\times V_{p,tissue}\right)\right]+\left[0.7\times V_{p,tissue}+{V_{wc,tissue}}/{F_{u,tissue}}\right]}{\left[K_{o:w}\times\left(V_{nl,plasma}+0.3\times V_{p,plasma}\right)\right]+\left[0.7\times V_{p,plasma}+{V_{wc,plasma}}/{F_{u,plasma}}\right]} \quad (11)$$

$$V_{Scsf}\frac{dC_{Scsf}}{dt} = \left(Q_{CRA\_SPL}\cdot C_{Ccsf}\right) - \left(Q_{SPL\_CRA}\cdot C_{Scsf}\right) - \left(Q_{SPL\_ABS}\cdot C_{Scsf}\right) \quad (7)$$

where the subscript S_{csf} represents the spinal CSF compartment. Mass balance for the cranial CSF compartment yields,

$$\begin{aligned} V_{Ccsf}\frac{dC_{Ccsf}}{dt} = {} & \left(Q_{SPL\_CRA}\cdot C_{Scsf}\right) - \left(Q_{CRA\_SPL}\cdot C_{Ccsf}\right) \\ & - \left(Q_{CRA\_ABS}\cdot C_{Ccsf}\right) + \left(Q_{cp}\cdot C_{Bb}\right) \\ & + \left(Q_{bulk}\cdot C_{ISF}\right) - \left(J_{CSF\_Efflux}\cdot fu_{Ccsf}C_{Ccsf}\right) \\ & + \left(J_{CSF\_Influx}\cdot fu_{Bb}C_{Bb}\right) \\ & + PS_{CSF}\left(fu_{Bb}C_{Bb} - fu_{Ccsf}C_{Ccsf}\right) \\ & + PS_{ISF\_CSF}\left(fu_{ISF}C_{ISF} - fu_{Ccsf}C_{Ccsf}\right) \end{aligned} \quad (8)$$

Finally, a mass balance about the brain blood compartment yields,

$$\begin{aligned} V_{Bb}\frac{dC_{Bb}}{dt} = {} & Q_{BRA}(C_{ART\_PL} - C_{Bb}) - Q_{BBB}\cdot C_{Bb} - Q_{cp} \\ & \cdot C_{Bb} + Q_{CRA\_ABS}\cdot C_{Ccsf} + Q_{SPL\_ABS}\cdot C_{Scsf} \\ & - \left(J_{ISF-Influx}\cdot fu_{Bb}C_{Bb}\right) \\ & + \left(J_{ISF-Efflux}\cdot fu_{ISF}C_{ISF}\right) \\ & - \left(J_{CSF-Influx}\cdot fu_{Bb}C_{Bb}\right) \\ & + \left(J_{CSF-Efflux}\cdot fu_{Ccsf}C_{Ccsf}\right) \\ & + PS_{ISF}\left(fu_{ISF}C_{ISF} - fu_{Bb}C_{Bb}\right) \\ & + PS_{CSF}\left(fu_{Ccsf}C_{Ccsf} - fu_{Bb}C_{Bb}\right) \end{aligned} \quad (9)$$

Blood barrier permeability values for the brain (PS_{ISF} and PS_{CSF}) are calculated based on diffusivity through a membrane barrier, given by,

$$PS_i = \frac{D_{drug}\cdot A_i}{\delta_i} \quad (10)$$

where D is drug-specific free diffusivity, A is surface area of the barrier and δ is membrane thickness. The surface area values used in simulation for the BBB and CSF-blood barrier are given in Table 2.The equation for the partition coefficients of the selected organs was obtained from literature [23]. The partition coefficient equation depends on the physicochemical properties of a drug and the water and protein content of the specific organ tissues.

where $K_{o:w}$ is the water: vegetable oil partition coefficient determined from the drug specific LogP, $V_{nl,tissue}$ and $V_{nl,plasma}$ are the volume fractions of neutral lipids in tissue and plasma respectively, V_p is the volume fraction of phospholipids, V_{wc} is the fractional water content and F_u is the unbound fraction. For this equation, tissue is considered as a mixture of water which contains neutral lipids, proteins, and phospholipids. The mixture is considered to be 70% water and 30% neutral lipids (by volume). This assumption comes from the fact that the hydrophilic/lipophilic balance value of phosphatidylcholine, which represents the commercial phospholipid, is reported as 14–15, with a value of 14 implying phospholipids in tissue behave as they would in a mixture of 70% water and 30% lipids. Poulin et al. provide a list of the fractional water, neutral lipid and phospholipid content of various organ tissues in rabbits, rats and mice [24, 25] which they obtained from literature.

While many of the parameters in our model were physiologically, anatomically or phenomenologically based, some parameters were not readily available in literature. Drug specific active transport and permeability parameters utilized in the enhanced brain model were calibrated for this reason. These values are provided in Table 2. While specific values for these parameters were not available, guidelines for their calibration were found in literature. In terms of active transport, morphine is a known Pgp (P-glycoprotein) substrate [26–28]. Pgp transporters actively efflux morphine from the brain capillary endothelium, acting as a barrier to BBB transport. We took this to indicate that active efflux of morphine should be greater than active influx, and thus implemented this constraint during calibration. The CSF-blood barrier is "leakier" than the BBB. As such, we applied two more constraints: (i) CSF-blood barrier permeability and active influx should be higher than that of the BBB for a given drug and (ii) active efflux should be lower than that of the BBB for a given drug. Permeability between brain ISF and tissue was calibrated so that the concentration of morphine

in brain tissue was approximately twice that of brain ISF, in accordance with experimental data found in literature [29].

Morphine-specific pharmacokinetics

Morphine is an opiate analgesic that acts directly on the central nervous system to relieve pain. Though morphine was discovered over 200 years ago, it remains the gold standard against which new post-operative and cancer-related pain relief is measured [30]. Morphine's ability to induce euphoric and relaxed feelings renders addiction potential high. Morphine can be administered orally, intravenously, intramuscularly, subcutaneously or rectally. Post-operative pain relievers, such as opioids, are typically administered into a patient's IV at regular intervals [31]. With this in mind, we selected morphine as the test case for our model, validating on IV bolus and IV infusion administration clinical data.

Morphine was assumed to instantaneously distribute to the entire venous volume. Morphine transport is characterized as previously discussed in the PBPK model description. The physicochemical properties of morphine (Table 3) dictate transport. Metabolism of morphine also contributes to PK changes and is considered in our model. Morphine metabolism has been reported in the liver [32–34] and brain [35, 36].

Morphine is primarily metabolized by glucuronidation via UGT2B7 [32]. Hepatic metabolism was reported to follow Michaelis–Menten kinetics,

$$R_{Liver} = \frac{V_{\max} \cdot C_{Liver} \cdot fu_{tissue}}{K_m + C_{Liver} \cdot fu_{tissue}} \quad (12)$$

where R_{Liver} is the reaction rate, fu_{tissue} is the unbound tissue fraction and V_{max} and K_m are kinetic constants. Cranial metabolism was assumed to follow first-order kinetics,

$$R_{Brain} = k_{brain\_metab} \cdot C_{Brain\_Tissue} \cdot fu_{tissue} \quad (13)$$

where k_{brain_metab} is the brain tissue metabolism rate constant. Drug metabolism can also occur within the brain interstitial fluid. The metabolic constant for brain ISF was assumed to be the same as that in brain tissue, as such data was not available in literature. Nearly all morphine and metabolites are excreted renally [37], of which only a small fraction is unchanged morphine. Unchanged morphine excretion is assumed to follow first-order kinetics,

$$E_{Kidney} = k_e \cdot C_{Kidney} \cdot fu_{tissue} \quad (14)$$

where k_e is the renal elimination rate constant.

Naloxone-specific pharmacokinetics

Naloxone is a μ-opioid antagonist with a high affinity for the μ-opioid receptors in the central nervous system. Naloxone reverses opioid analgesic effects by binding to opioid receptors and inhibiting typical opioid actions including analgesia, euphoria, sedation and respiratory depression [38]. Naloxone is typically administered intravenously, intramuscularly and subcutaneously in hospital settings and intranasally in prehospital settings [39]. Naloxone is currently the primary antidote to opioid drug overdose.

With these considerations in mind, we validated our integrated PBPK and PD model using IV bolus administered naloxone. The naloxone dose was assumed to distribute instantaneously to the entire venous volume, same as morphine. Naloxone transport was also described by the PBPK model discussed previously in this paper. The

Table 3 Physicochemical Properties of Morphine

Parameter[a]	Value	Unit
Molecular weight	285.34	g/mol
LogP	0.77	–
Unbound fraction: plasma (fu_p)	0.62	–
Unbound fraction: tissue (fu_t)	0.45	–
Blood to plasma partitioning ($Kp_{blood\text{-}cell}$)	1.08	–
M6G maximum rate of reaction ($V_{m,\ M6G}$)	1917	pmol/min/mg microsomal protein
Morphine metabolite M6G Michaelis–menten constant ($K_{m,\ M6G}$)[b]	1120	μmol/L
M6G Maximum rate of reaction ($V_{m,\ M3G}$)	9250	pmol/min/mg microsomal protein
Morphine metabolite M3G Michaelis–menten constant ($K_{m,\ M3G}$)[b]	1110	μmol/L
Renal clearance (k_e)	8	L/h

[a] [32] compiled this collection of parameters from literature

[b]Taken from [76]

Table 4 Physicochemical Properties of Naloxone

Parameter	Value	Unit
Molecular weight[a]	327.375	g/mol
LogP[a]	2.09	–
Unbound fraction: plasma[b] (fu_p)	0.62	–
Unbound fraction: tissue (fu_t)	0.77	–
Blood to plasma partitioning[b] ($Kp_{blood\text{-}cell}$)	1.08	–

[a]From [39]

[b]From [41]

physicochemical properties of naloxone dictate transport (Table 4).

In addition to transport, the naloxone metabolism contributes to PK changes. Naloxone metabolism has been reported in the liver [40, 41], intestines [41] and brain [35]. Intestinal and hepatic metabolism were shown to follow Michaelis–Menten kinetics (see Eq. 12). The metabolic constants for intestinal and hepatic metabolism were obtained from rat studies [41] and so were scaled by microsomal protein content to obtain parameters to fit our human model. Cranial metabolism was assumed to follow first-order kinetics (see Eq. 13). The brain metabolism rate constant was calculated by the summing the brain tissue metabolism rate constants reported in literature [35]. Naloxone excretion also contributes to PK changes. Naloxone is primarily excreted in urine. Naloxone excretion is assumed to follow first-order kinetics, same as morphine (see Eq. 14).

Pharmacodynamic Models of Morphine and Naloxone

The μ-opioid receptor (R) is the primary target for morphine binding where it acts as an agonist to elicit its analgesic effect. Excessive doses of morphine can trigger other undesired effects such as euphoria, nausea, respiratory depression and death [38]. A prolonged period of respiratory depression can lead to respiratory arrest and eventually death. Naloxone has a high affinity for the μ-opioid receptor and works to reverse respiratory depression through competitive binding and displacement of bound opioids [42].

Our pharmacodynamic model characterizes respiratory depression as a function of morphine-receptor binding similar to [43]. Morphine and naloxone receptor binding is characterized by equilibrium equations,

$$\frac{d[MR]}{dt} = k_{on,M}[M][R] - k_{off,M}[MR] \tag{15}$$

And

$$\frac{d[NR]}{dt} = k_{on,N}[N][R] - k_{off,N}[NR] \tag{16}$$

where k_{on} and k_{off} are receptor equilibrium rate constants. The total number of receptors (R_t) is

$$R_t = [R] + [MR] + [NR] \tag{17}$$

where, [R] is the number of unbound receptors. Substituting Eq. 17 in Eq. 15 and Eq. 16, and normalizing by R_t, gives

$$\frac{d[\overline{MR}]}{dt} = k_{on,M}[M]\left[1 - \overline{MR} - \overline{NR}\right] - k_{off,M}\left[\overline{MR}\right] \tag{18}$$

And

$$\frac{d[\overline{NR}]}{dt} = k_{on,N}[N]\left[1 - \overline{MR} - \overline{NR}\right] - k_{off,N}\left[\overline{NR}\right] \tag{19}$$

where $[\overline{MR}] = \frac{[MR]}{R_t}$ and $[\overline{NR}] = \frac{[NR]}{R_t}$ are the normalized concentration of receptor-bound morphine and naloxone. Time dependent solutions to Eqs. 18 and 19 act as input for the PD equation.

Olofsen et al. [43] went a step further to simplify the above differential Eqs. (18 and 19) into algebraic expressions by assuming that $k_{off,N}$ (naloxone dissociation constant) is large [44]. With this assumption and at steady state, Eq. 19 reduces to,

$$[\overline{NR}] = \frac{[N]\left[1 - \overline{MR}\right]}{k_{D,N} + [N]} \tag{20}$$

where $k_{D,N} = \frac{k_{off,N}}{k_{on,N}}$ and $k_{D,M} = \frac{k_{off,M}}{k_{on,M}}$

Substituting Eq. 20 into 21 and assuming steady state we obtain,

$$[\overline{MR}] = \frac{[M][1 - X]}{k_{D,M} + [M][1 - X]} \tag{21}$$

and $X = \frac{[N]}{k_{D,N}+[N]}$

Values for the binding constants $k_{D,M}$ and $k_{D,N}$ are provided in Table 5. The values input for [M] and [N] are the respective total brain ISF concentrations. This gives us two approaches to modeling receptor binding, and the results for both model approaches are presented in the RESULTS section.

Table 5 Parameters for PD model

Parameter	Value[a]	Unit
Naloxone receptor binding ratio ($k_{D,N}$)	1.840	nmol/L
Morphine receptor binding ratio ($k_{D,M}$)	78.6*	nmol/L

[a] Parameter values taken from literature [32]

*Calibrated within SD of $k_{on,M}$ and $k_{off,M}$

Drug efficacy was evaluated on a measurable endpoint, the fractional modification of ventilation (V_E). Ventilation (units of L/min) is calculated by multiplying the respiratory rate (breaths/min) by the tidal volume (lung volume representing the normal volume of air displaced between inhalation and exhalation in the absence of excess effort). The baseline values for tidal volume and respiratory rate provided in the literature were 1.3 L and 19.1 breaths/min, respectively. The PD model for ventilation modification was assumed to depend on [MR] as proposed previously [43], and given by,

$$V_E = V_0 \cdot \left(1 - \left[\overline{MR}\right]\right) \tag{22}$$

where, V_0 is the baseline respiratory/ventilation rate. Also, since $\left[\overline{MR}\right]$ is normalized, i.e. $\left(0 < \left[\overline{MR}\right] < 1\right)$, it follows that $\left(0 < V_E < V_0\right)$.

All simulations were performed using an in-house developed, multiscale, multiphysics open source software, Computational Biology (CoBi) Tools. These tools have been developed and validated under several projects with DoD, NIH, CDC, FDA, NASA and US bio-pharma industry [45–47]. The model code is provided in Online Resource 1.

Results

Validation of morphine PBPK Model on human clinical data

The morphine PBPK model described above was used to simulate IV bolus and IV infusion administration of morphine in humans. Concentration–time profiles from simulations were compared to the clinical observations in human-studies to validate the model. PBPK model validation criteria included (i) matching the general trend of the clinical data, (ii) model overlap within the clinical data error bars (when available), (iii) model AUC falling within the reported AUC range from clinical data (when available), (iv) model drug half-life lying within the reported clinical data range. Models were considered validated if they matched criteria (i) and at least one of the other three criteria. The same criteria was used to validate the PBPK model on naloxone. A brain ISF to brain tissue concentration ratio of approximately 2 at Cmax [29] was used to validate the brain model for morphine.

For the first model validation, simulated total plasma concentration after IV bolus administration of 5.64 mg of morphine was compared to the clinical observations from [48]. This population-based clinical study was performed on 8 healthy, young volunteers (4 males; 4 females) with an average weight of 70.5 kg. The average weight was considered in the model simulation for scaling of physiological parameters as identification of individualized PK data and weight was not possible. Figure 4 presents both the clinically observed and model simulated morphine plasma concentration profiles as a function of time. The simulation results are well within the range of the concentrations observed in the clinical data set for the population and follow the general trend for morphine distribution in unbound plasma.

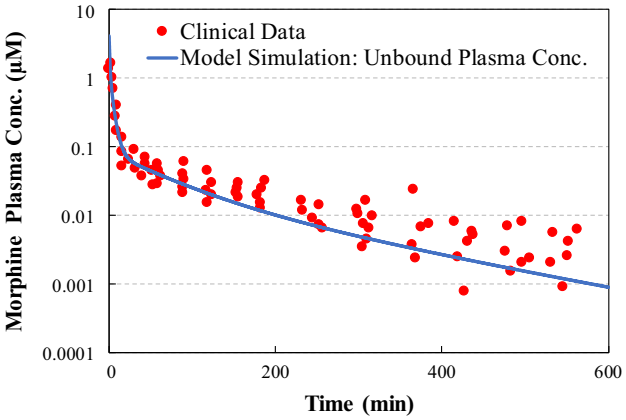

Fig. 4 Total morphine concentration in arterial plasma (observed vs. simulated) after IV bolus administration of 5.64 mg morphine. The experimental data was reported by [48], presented as a collection of individual data

Another simulation was performed to compare and validate the morphine PBPK model for IV infusion administration. Figure 5 shows the simulated arterial plasma concentration compared to observed data [49] after an 8.8 mg IV infusion of morphine given over 7 min. In this clinical study, morphine was administered intravenously in 13 subjects with a mean weight of 74 kg. All volunteers were young and healthy in the age group of 22–45 years of age. Simulated profile during the infusion

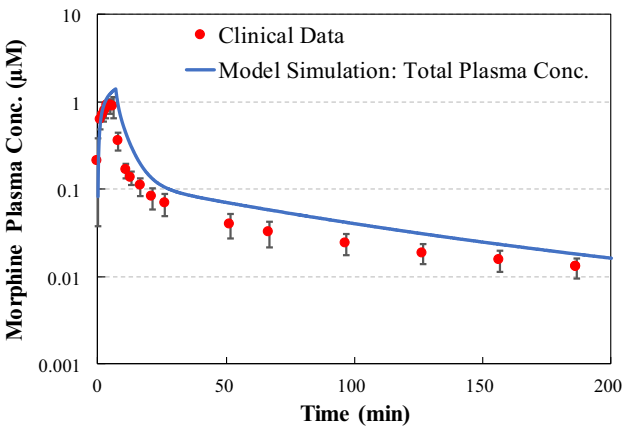

Fig. 5 Total morphine concentration in arterial plasma (observed vs. simulated) after IV infusion of 8.8 mg morphine over 7 min. The experimental data was reported by [49], presented as the mean ± SD

phase matches very well with experimental data. The distribution phase morphine concentrations predicted by the PBPK model are slightly higher than observed data. However, it must be noted that the concentration is plotted on a log scale and the difference in the observed and simulated concentrations is of fairly low magnitude (0.02–0.5 μM).

In order to validate the 5-compartment brain model integrated into our PBPK model, we scoured literature for experimental data regarding morphine concentrations in brain tissue. A study was conducted on a 52-year-old male patient with a severe brain injury, in which intracerebral microdialysis was used to measure the morphine concentration in uninjured and injured brain regions [50]. This patient was administered 10 mg of morphine by IV infusion given over 10 min. Infusion administration was achieved in simulation via a constant stepwise increase in administered drug concentration, which was calculated using the total administered concentration and number of simulation time steps occurring over the infusion time period. This study did not specify the weight of the patient, and as such, the average weight of Caucasian adult males 20 years of age and older was used. The average weight found in literature was around 90 kg [51]. Predicted unbound brain tissue, ISF and plasma concentrations were plotted with respect to time and compared with unbound brain tissue morphine concentration data from microdialysis samples [50] (Fig. 6). Plasma concentration during the infusion and distribution phases match well with experimental data, similar to the previous simulation (Fig. 5). Additionally, brain tissue and brain ISF concentrations match well with experimental data. Brain tissue concentration is approximately twice that of brain ISF, similar to reported experimental data [29].

A second set of clinical data for brain morphine concentration was used for brain model validation [52]. Similar to the previous data set, unbound brain and plasma morphine concentration data following 10 mg IV infusion over 10 min were presented. In Fig. 7a, b, the reported clinical data are presented for two different patients with no data for their weights. A weight of 90 kg was again assumed for simulation. Model prediction for plasma concentration falls in between the two data sets. Model prediction for brain tissue and brain ISF also match well with experimental data. Overall, for both routes of administration (IV bolus and IV infusion), the morphine PBPK and advanced brain models predict PK profiles reasonably well.

Validation Naloxone PBPK model results on human clinical data

A similar PBPK model for human was developed for naloxone using the same framework as for the morphine PBPK model. The physicochemical and ADME properties of naloxone were incorporated into this framework to construct a naloxone-specific PBPK model. Similar to the morphine PBPK model, this model has the ability to simulate IV bolus and IV infusion administration.

Validation of the naloxone model was performed using clinical data from literature [53], from a study involving 12 healthy subjects with 6 males (mean weight of 77.7 kg) and 6 females (mean weight of 59.0 kg). In this simulation, the human weight is considered to be 68.5 kg (average of 12 subjects). Simulated and observed plasma concentration–time profiles of naloxone are compared in Fig. 8 for IV bolus administration of 0.8 mg of naloxone. The simulated general trend for the naloxone plasma PK profile matches

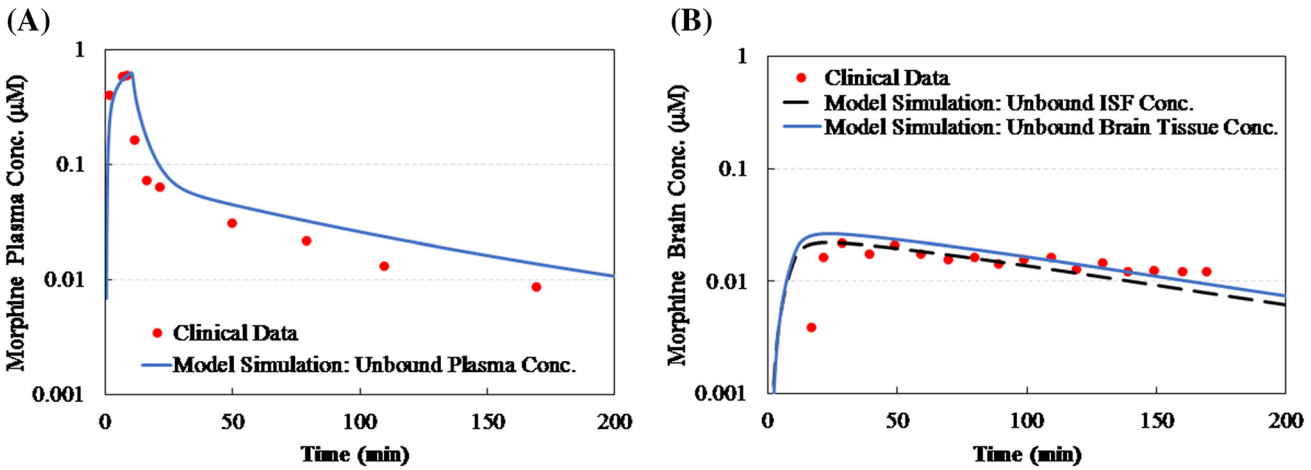

Fig. 6 Unbound morphine concentration in **a** blood and **b** brain tissue and brain blood compartments (observed vs. simulated) after intravenous infusion of 10 mg morphine over 10 min. The clinical data was reported by [50], presented as individual data

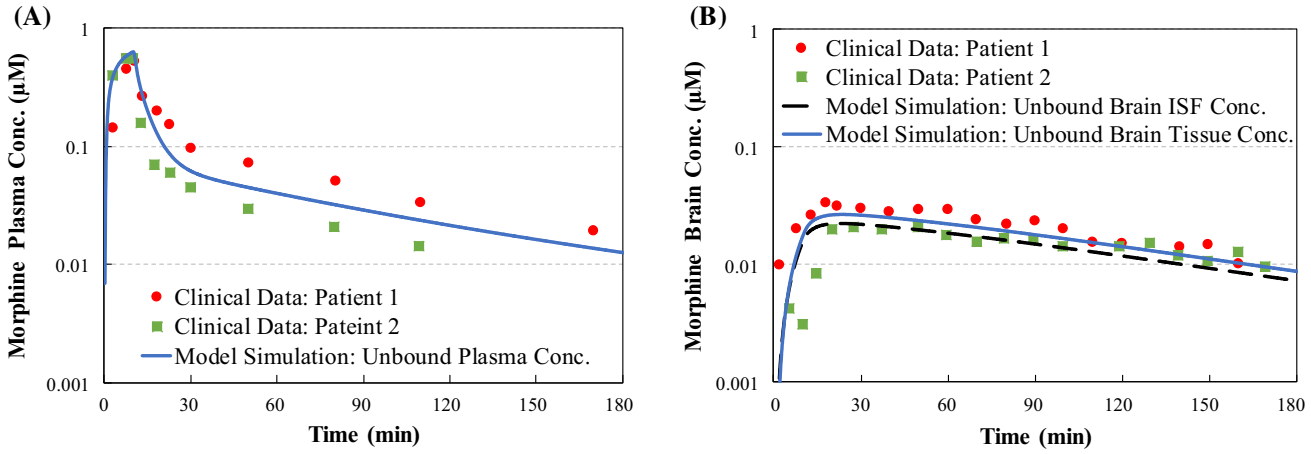

Fig. 7 Unbound morphine concentration in **a** arterial plasma and **b** brain tissue compartments (observed vs. simulated) after intravenous infusion of 10 mg morphine over 10 min. The observed clinical data was reported by [52], presented as two individual data sets (red and green)

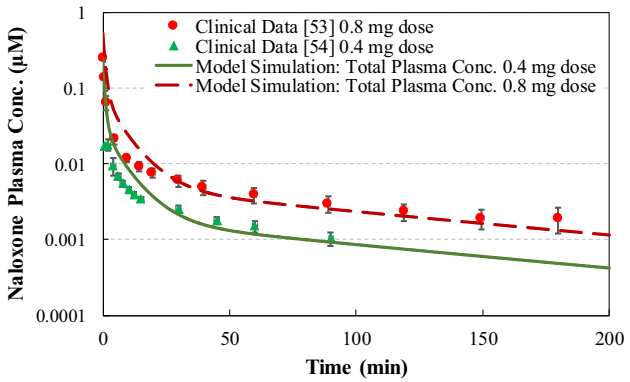

Fig. 8 Serum plasma naloxone concentration (observed) versus simulated total plasma concentration after IV bolus administration of 0.8 and 0.4 mg naloxone. The observed data for the 0.8 mg dose is from [53], presented as the mean ± standard error of the mean (SEM). The observed data for the 0.4 mg dose was reported by [54], presented as the mean ± SD

well with that from reported data and predicted concentrations are comparable with clinical data.

Additional naloxone model validation was performed using clinical data from literature [54]. Figure 8 shows the comparison of simulated plasma profiles to clinical data following IV bolus injection of 0.4 mg naloxone. The reported clinical data was collected in 8 healthy volunteers. No information was provided regarding the weight of the volunteers, and as such, a 70 kg weight was assumed for simulation. The simulated results are slightly higher than clinical data during the absorption phase of the PK profile while the distribution phase matches well with clinical data. Clinical data demonstrated a rise in naloxone plasma concentration following IV bolus administration which was not observed in the other naloxone data set. Increase in concentration is also extremely uncommon in cases of IV bolus injection. This may explain the slight differences between model predictions and clinical data seen in the first 20 min of the PK profile.

Both the morphine and naloxone PBPK predictive simulation results are comparable to the clinical observations in all 6 comparison/validation cases.

Morphine–Naloxone PK/PD model of respiratory depression response

The PD models were each in turn incorporated into the combined PBPK model of morphine and naloxone. The model results were compared with two clinical cases and two simulation studies for validation of the combined PBPK-PD model.

Clinical studies for both cases were performed by [43]. Two groups of 8 healthy volunteers participated in the study. In simulation of both cases, the human weight was assumed to be 69 kg, the mean weight of the healthy volunteers who participated in the study.

Study I

In this study, 8 healthy volunteers intravenously received morphine (0.15 mg/kg) at time t = 0, followed by a placebo at 30 min. An IV bolus administration of the indicated morphine dose at time t = 0 was simulated for comparison. Nothing was administered to represent the placebo in simulation. Comparison of the clinical and model results is shown Fig. 9a.

Study II

In the second study, another group of 8 healthy volunteers were intravenously dosed with 0.15 mg/kg of morphine at t = 0 min, followed by a 0.2 mg dose of naloxone at time

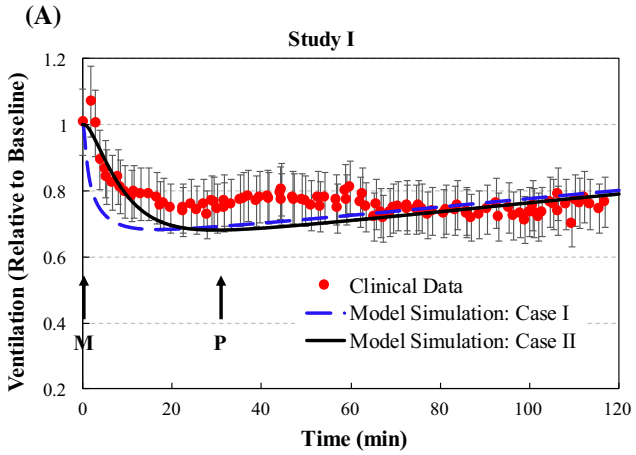

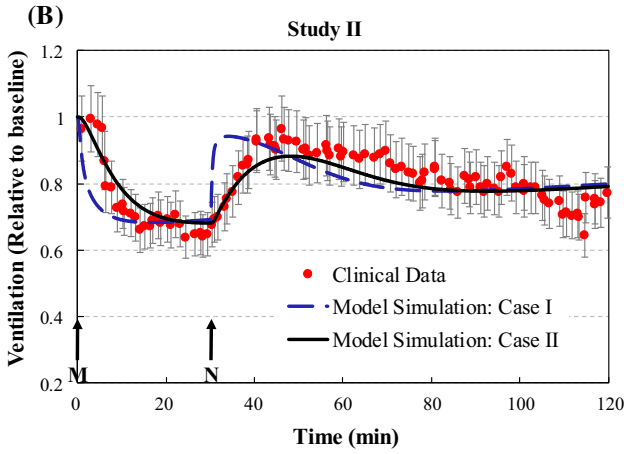

Fig. 9 Pharmacodynamic response in terms of respiratory depression (ventilation) relative to the baseline for **a** morphine administration followed by placebo administration and **b** morphine administration followed by naloxone administration. The observed data was reported by [43], presented as the mean ± SEM

t = 30 min. An IV bolus administration of the indicated morphine dose at time t = 0 was simulated for comparison. At time t = 30 min an IV bolus dose of 0.2 mg naloxone was administered in the simulation. Comparison of simulated and clinical data are shown in Fig. 9b.

Two approaches were taken to simulate the opioid receptor binding kinetics associated with the PD model.

Model I

Simulation was performed using the simplified algebraic Eqs. (20 and 21) to characterize morphine and naloxone receptor binding. This approach is similar to the model simulation approach discussed by [43].

Model II

Simulation was performed using the ODEs (18 and 19) to characterize morphine and naloxone receptor binding. These ODEs were solved simultaneously. Equations 18 and 19 require value input for $k_{on,N}$ and $k_{off,N}$ and $k_{on,M}$ and $k_{off,M}$. These values for were taken from literature [40] and also used to calculate $k_{D,M}$ values used in Model I.

The model predicts the PK-PD profile of respiratory depression relative to baseline, where pre-drug ventilation is represented by baseline = 1.

We also checked the model to ensure that the administration of naloxone alone did not alter respiratory depression. Figure 10 demonstrates the model's lack of PD response to binding of naloxone to opioid receptors in the absence of morphine.

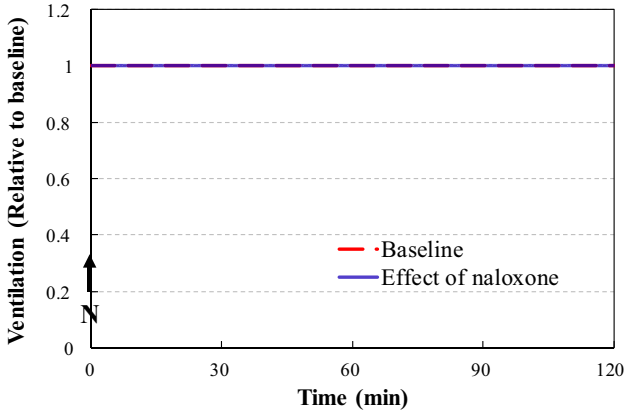

Fig. 10 Naloxone administration alone does not impact respiratory depression

Discussion

Morphine exerts its analgesic effects for the relief of severe pain through activation of opioid receptors (ORs), a large superfamily of G protein-coupled receptors (GPCRs). Activation of ORs by morphine results in both pharmacological effects (analgesia) as well as undesired side effects including constipation, nausea, vomiting, urinary retention, pruritus, muscular rigidity, miosis, respiratory depression [43] and, after prolonged use, withdrawal, tolerance and addiction. Clinical pharmacodynamic effects of morphine can be monitored using physiological responses such as cortical electroencephalographic (EEG) measurements, miosis (decrease of ocular pupil diameter) and respiratory depression. PK simulations provide concentration profiles in brain tissues as input for the PD model of opioid binding to neuronal receptors and the resultant physiological response profiles. The goal of this paper was to develop a

first principles-based PBPK model and integrated minimalistic PD model to characterize the disposition and competitive interaction of morphine and naloxone with neural ORs and a simple model of respiratory depression. These models were used to evaluate the protective effects of naloxone administered after morphine intoxication. The uniqueness of the presented model is in the integration of whole-body PBPK with anatomically resolved CNS compartments, drug ligand binding kinetics to ORs and the resultant respiratory responses.

Mathematical modeling of drug PK and PD is a cost and time effective way to evaluate the effects of changing drug related parameters (dose, route of administration, etc.). Mechanistic modeling can provide insight into important factors impacting PK and PD variability. Development of these models with appropriate resolution of drug target tissues is critical. In the case of opioid PK and PD modeling, a high-resolution PBPK model of the brain is necessary, due to its complex anatomical and physiological structures and mechanisms. Various factors such as local metabolism, transport through the blood–brain and blood-CSF-barriers, passive permeability, CSF circulation, etc. play a significant role in the distribution of these drugs in brain. On the other hand, excessive sub-compartmentalization of the brain often requires extensive calibration of parameters, especially for human model. The 4-compartment brain model provides an excellent balance in complexity and measurable parameters. The use of brain microdialysis and novel imaging technology provide improved insight into regional brain concentrations. However, these are highly sensitive to the techniques used for concentration measurement.

The PBPK models for morphine and naloxone were validated for IV bolus and IV infusion administration by comparison of the simulated concentration–time profiles with clinical data in healthy volunteers. In general, the model predictions for morphine and naloxone PK were in good agreement with the published data (Figs. 1, 2, 3, 4, 5, 6). Biphasic and rapid distribution of both morphine and naloxone concentrations in plasma were observed and found to be in agreement with the presented clinical data. This is in agreement with reports of rapid analgesia onset associated with IV morphine administration [55]. Greater differences between simulation and clinical data for morphine were observed for IV infusion administration, particularly during the absorption and distribution phases. In these cases, the drip-rate accuracy can be significantly impacted when subjects change positions, and could cause initial differences [56]. Moreover, marked inaccuracies in IV fluid infusion rates are common [57].

Brain tissue or fluid sampling is not performed in healthy volunteers, due to the invasive nature of sampling techniques. Despite the collection of samples from what is deemed a "healthy" part of a patient's injured brain, the transport and metabolism of drugs in the brain can still be impacted. These differences could explain the small differences observed between clinical data and our model predicted PK profiles of morphine in the brain. The importance of sampling location can also be observed through the implementation of our model. Comparison of the clinical data [50] to model predicted brain blood concentration (not shown) demonstrated a poor fit. However, comparison of the clinical data with the morphine brain tissue and ISF concentrations demonstrates a much better fit that matches the clinical profile trend very well.

Clinical pharmacokinetic parameters ($t_{1/2}$, C_{max} and AUC) were also compared with those determined from simulation (Table 6). The values of these parameters depend on the dose amount and duration and as such were compared individually for each administration scenario. The maximum peak concentration (C_{max}) was slightly overpredicted in all comparisons. One of the plausible reasons for overprediction could be lack of a continuous sampling data set in clinical studies. These C_{max} values may have matched even more closely if clinical samples were taken at the time at which C_{max} occurred in simulation. The C_{max} for [54] was much higher in simulation as compared to the clinical study. But, the clinical data looks like an IV infusion curve where the concentration starts dropping down after 1–2 min, whereas the study mentions IV bolus administration of naloxone. So, the drastic difference between C_{max} can also be attributed to some discrepancies in the clinical methods as well. The terminal elimination phase half-lives generally matched very well with the observed clinical data, further validating the PK formulation of the model. AUC were calculated using

Table 6 Comparison of pharmacokinetic parameters ($t_{1/2}$, C_{max} and AUC) for morphine and naloxone in blood from clinical data and corresponding model prediction

Source	$t_{1/2}$ (h)	C_{max} (μM)	AUC (μM/h)
Morphine pharmacokinetic parameters			
[48]	2.8	2.10	*0.1822–0.3371
Model	2.01	4.12	*0.3185
[49]	1.604 (± 0.068)	0.92–1.08	Data not reported
Model	1.24	1.40	0.3375
Naloxone pharmacokinetic parameters			
[53]	2.52 (0.785–5.22)	0.248	Data not reported
Model	1.61	0.648	0.0258
[54]	1.25 (± 0.216)	0.0422	0.0031–0.0095
Model	1.34	0.237	0.00837

*This AUC is calculated from time = 0 to infinity. All AUCs are calculated up to the last data point

trapezoidal rule and were well within the range given by the clinical studies.

The PD model of opioid-OR interaction was partially validated on available clinical data of human respiratory depression after morphine IV delivery and recovery following naloxone IV administration. Figure 9a shows the experimentally measured [43] and model predicted respiratory depression (ventilation) relative to the physiological baseline. Considering that model II was a simple algebraic correlation, assuming instantaneous response to OR-bound morphine, the model agrees well with the measured profiles of rapid depression and slow recovery. Moreover, a rapid response or onset of action is reported for IV administration of morphine [55]. Additionally, peak onset of action is reported around 20 min post IV administration [55] and is in good agreement with predicted peak respiratory depression levels. Figure 9b presents simulation results for naloxone reversal of morphine-induced respiratory depression and compares clinical data to model predicted respiratory depression. For the first 30 min, after morphine delivery, the predicted respiratory depression profile is the same as in the previous case. However, the experimental data for the first 30 min period show large differences, despite the same protocol of morphine delivery (0.15 mg/kg IV bolus morphine administration at $t = 0$). Unfortunately, the plasma PK for morphine was not available, and therefore it is difficult to attribute the differences to a specific cause. Good agreement between the predicted and experimental respiratory depression response using model II was observed. Note the characteristic bi-phasic response—first fast recovery (for the period of approximately 10 min after naloxone infusion) followed by slow recovery up to 120 min. This is in agreement with naloxone's reported onset of action of 1–2 min [39]. Comparing the results of PD Model I (equilibrium bound naloxone assumption, similar to [43]) and Model II (dynamic model of naloxone binding kinetics) it can be seen that the dynamic model provides better agreement with clinical data.

The model presented in this study has several limitations which could be improved. First and foremost is the need for experimental measures and/or efforts to validate active and passive transport contributions of morphine and naloxone at the BBB and CSF-blood barrier. The current model, uses IV naloxone administration only, but should be extended to account for intramuscular (IM) injection and nasal spray delivery for the reversal of opioid effects in cases of overdose. Such advancements will require the development and validation of a naloxone absorption depot model (IM) and a nasal/olfactory epithelial barrier model. A population PBPK model including pediatric subjects, possible gender-dependent effects and statistical analysis of model parameter sensitivity should be pursued. The simple model of respiratory physiology could be extended to simulate noninvasive biomarker kinetics in plasma (e.g. pulse oximetry) and breath (breathing pattern and exhaled gases). The model could also be further extended to study different combinations of opioid receptor agonists and antagonists. Multidisciplinary efforts of model-based development of an 'ideal' reversal agent that is not influenced by the opioid's receptor kinetics, does not interfere with analgesia and has a rapid onset and prolonged protective effect should be pursued.

Conclusions

The present quasi-equilibrium PD model, relating the respiratory response to the brain bound morphine concentration, can be further improved by involving mechanistic models of opioids receptor signaling pathways, biomarkers kinetics and models of neurocognitive and physiological responses. Opioids mediate analgesia as well as adverse effects in both inflamed tissue and in the central nervous system via G-protein coupled opioid receptors (GPCRs), for which advanced signaling pathways and ligand binding kinetics have been established [58–60]. Such models could be used for the development of GPCR biased ligands that activate desired G-protein coupled analgesia without β-arrestin recruitment. The present simple respiratory response model could be replaced by more advanced respiration control models [61, 62]. While respiratory depression is the defining endpoint of opioid toxicity [63], mathematical models of accompanying endpoints, such as pupillometry, EEG measurements could be also included. However, one must be careful when considering miosis as a measurable endpoint for opioid toxicity coupled with naloxone recovery, as naloxone has also been shown to induce miosis in healthy and opiate addict populations [64].

Acknowledgements This research was funded internally by CFD Research Corporation's IR&D. The authors greatly appreciate the assistance of Dr. ZJ Chen and Mr. Alex Boyer in assisting with model development and implementation of our model in an online format, respectively. We also thank Ms. Lindsey Maurel for her contribution of artwork. We would also like to extend our gratitude to the reviewers for providing keen insights and suggestions with which the model was able to be improved.

References

1. Skolnick P (2018) The opioid epidemic: crisis and solutions. Annu Rev Pharmacol Toxicol 58:143–159. https://doi.org/10.1146/annurev-pharmtox-010617-052534
2. Volkow ND, McLellan AT (2016) Opioid abuse in chronic pain—misconceptions and mitigation strategies. N Engl J Med 374:1253–1263. https://doi.org/10.1056/NEJMra1507771

3. Mendelson J, Flower K, Pletcher M, Galloway GP (2008) Addiction to prescription opioids: characteristics of the emerging epidemic and treatment with buprenorphine. Exp Clin Psychopharmacol 16:435–441. https://doi.org/10.1037/a0013637
4. McGregor AJ (2018) The opioid epidemic: overcoming challenges by using a sex and gender lens. Clin Ther 40:188–189. https://doi.org/10.1016/j.clinthera.2018.01.007
5. Vashishtha D, Mittal ML, Werb D (2017) The North American opioid epidemic: current challenges and a call for treatment as prevention. Harm Reduct J 14:7. https://doi.org/10.1186/s12954-017-0135-4
6. Cascone S, Lamberti G, Piazza O, Abbiati RA, Manca D (2018) A physiologically-based model to predict individual pharmacokinetics and pharmacodynamics of remifentanil. Eur J Pharm Sci 111:20–28. https://doi.org/10.1016/j.ejps.2017.09.028
7. Kalluri HV, Zhang H, Caritis SN, Venkataramanan R (2017) A physiologically based pharmacokinetic modelling approach to predict buprenorphine pharmacokinetics following intravenous and sublingual administration. Br J Clin Pharmacol 83:2458–2473. https://doi.org/10.1111/bcp.13368
8. Lötsch J (2005) Pharmacokinetic-pharmacodynamic modeling of opioids. J Pain Symptom Manag 29:S90–103. https://doi.org/10.1016/j.jpainsymman.2005.01.012
9. Shankaran H, Adeshina F, Teeguarden JG (2013) Physiologically-based pharmacokinetic model for Fentanyl in support of the development of provisional advisory levels. Toxicol Appl Pharmacol 273:464–476. https://doi.org/10.1016/j.taap.2013.05.024
10. Yassen A, Olofsen E, van Dorp E, Sarton E, Teppema L, Danhof M, Dahan A (2007) Mechanism-based pharmacokinetic-pharmacodynamic modelling of the reversal of buprenorphine-induced respiratory depression by naloxone. Clin Pharmacokinet 46:965–980. https://doi.org/10.2165/00003088-200746110-00004
11. Ahmed S, Graupner M, Gutkin B (2009) Computational approaches to the neurobiology of drug addiction. Pharmacopsychiatry 42:S144–S152. https://doi.org/10.1055/s-0029-1216345
12. Ball K, Bouzom F, Scherrmann J-M, Walther B, Declèves X (2012) Development of a physiologically based pharmacokinetic model for the rat central nervous system and determination of an in vitro–in vivo scaling methodology for the blood–brain barrier permeability of two transporter substrates, morphine and oxycodone. J Pharm Sci 101:4277–4292. https://doi.org/10.1002/jps.23266
13. Yamamoto Y, Välitalo PA, Huntjens DR, Proost JH, Vermeulen A, Krauwinkel W, Beukers MW, van den Berg D-J, Hartman R, Wong YC, Danhof M, van Hasselt JGC, de Lange ECM (2017) Predicting drug concentration-time profiles in multiple CNS compartments using a comprehensive physiologically-based pharmacokinetic model. CPT Pharmacomet Syst Pharmacol 6:765–777. https://doi.org/10.1002/psp4.12250
14. Borjkhani M, Bahrami F, Janahmadi M (2018) Computational modeling of opioid-induced synaptic plasticity in hippocampus. PLoS ONE 13:e0193410. https://doi.org/10.1371/journal.pone.0193410
15. de Carvalho LAV, de Azevedo LO (2000) A model for the cellular mechanisms of morphine tolerance and dependence. Math Comput Model 32:933–953. https://doi.org/10.1016/S0895-7177(00)00180-1
16. Christie MJ (2008) Cellular neuroadaptations to chronic opioids: tolerance, withdrawal and addiction. Br J Pharmacol 154:384–396. https://doi.org/10.1038/bjp.2008.100
17. Dumas EO, Pollack GM (2008) Opioid tolerance development: a pharmacokinetic/pharmacodynamic perspective. AAPS J 10:537. https://doi.org/10.1208/s12248-008-9056-1
18. Evans WE, Schentag JJ, Jusko WJ (1992) Applied pharmacokinetics: principles of therapeutic drug monitoring. Appl Ther Incorp 1:1. https://doi.org/10.1002/bdd.2510030315
19. Peters SA (2012) Physiologically-based pharmacokinetic (PBPK) modeling and simulations: principles, methods, and applications in the pharmaceutical industry. Wiley, New York
20. Thompson MD, Beard DA (2011) Development of appropriate equations for physiologically based pharmacokinetic modeling of permeability-limited and flow-limited transport. J Pharmacokinet Pharmacodyn 38:405–421. https://doi.org/10.1007/s10928-011-9200-x
21. Zhang F, Tagen M, Throm S, Mallari J, Miller L, Guy RK, Dyer MA, Williams RT, Roussel MF, Nemeth K, Zhu F, Zhang J, Lu M, Panetta JC, Boulos N, Stewart CF (2011) Whole-body physiologically based pharmacokinetic model for nutlin-3a in mice after intravenous and oral administration. Drug Metab Dispos Biol Fate Chem 39:15–21. https://doi.org/10.1124/dmd.110.035915
22. Gaohua L, Neuhoff S, Johnson TN, Rostami-Hodjegan A, Jamei M (2016) Development of a permeability-limited model of the human brain and cerebrospinal fluid (CSF) to integrate known physiological and biological knowledge: estimating time varying CSF drug concentrations and their variability using in vitro data. Drug Metab Pharmacokinet 31:224–233. https://doi.org/10.1016/j.dmpk.2016.03.005
23. Berezhkovskiy LM (2004) Volume of distribution at steady state for a linear pharmacokinetic system with peripheral elimination. J Pharm Sci 93:1628–1640. https://doi.org/10.1002/jps.20073
24. Poulin P, Krishnan K (1995) A biologically-based algorithm for predicting human tissue: blood partition coefficients of organic chemicals. Hum Exp Toxicol 14:273–280. https://doi.org/10.1177/096032719501400307
25. Poulin P, Theil F-P (2000) A priori prediction of tissue:plasma partition coefficients of drugs to facilitate the use of physiologically-based pharmacokinetic models in drug discovery. J Pharm Sci 89:16–35. https://doi.org/10.1002/(SICI)1520-6017(200001)89:1%3c16:AID-JPS3%3e3.0.CO;2-E
26. Löscher W, Potschka H (2005) Blood-brain barrier active efflux transporters: ATP-binding cassette gene family. NeuroRx 2:86–98. https://doi.org/10.1602/neurorx.2.1.86
27. Chaves C, Remião F, Cisternino S, Declèves X (2017) Opioids and the blood-brain barrier: a dynamic interaction with consequences on drug disposition in brain. Curr Neuropharmacol 15:1156–1173. https://doi.org/10.2174/1570159X15666170504095823
28. Mercer SL, Coop A (2011) Opioid analgesics and P-glycoprotein efflux transporters: a potential systems-level contribution to analgesic tolerance. Curr Top Med Chem 11:1157–1164. https://doi.org/10.2174/156802611795371288
29. Stain-Texier F, Boschi G, Sandouk P, Scherrmann J-M (1999) Elevated concentrations of morphine 6-beta-D-glucuronide in brain extracellular fluid despite low blood–brain barrier permeability. Br J Pharmacol 128:917–924. https://doi.org/10.1038/sj.bjp.0702873
30. Bryan J (2018) Even today, morphine remains a popular opioid analgesic for cancer-related pain. Lung Cancer 15:05. https://doi.org/10.1111/bcp.12008
31. Mayo Clinic Staff (2017) Pain medications after surgery. In: Mayo Clin. http://www.mayoclinic.org/pain-medications/art-20046452
32. Emoto C, Fukuda T, Johnson T, Neuhoff S, Sadhasivam S, Vinks AA (2017) Characterization of contributing factors to variability in morphine clearance through PBPK modeling implemented with OCT1 transporter. CPT Pharmacomet Syst Pharmacol 6:110–119. https://doi.org/10.1002/psp4.12144

33. Smith HS (2009) Opioid metabolism. Mayo Clin Proc 84:613–624. https://doi.org/10.1016/S0025-6196(11)60750-7
34. Soleimanpour H, Safari S, Shahsavari Nia K, Sanaie S, Alavian SM (2016) Opioid drugs in patients with liver disease: a systematic review. Hepat Mon. https://doi.org/10.5812/hepatmon.32636
35. Wahlström A, Winblad B, Bixo M, Rane A (1988) Human brain metabolism of morphine and naloxone. Pain 35:121–127. https://doi.org/10.1016/0304-3959(88)90219-9
36. Yamada H, Ishii K, Ishii Y, Ieiri I, Nishio S, Morioka T, Oguri K (2003) Formation of highly analgesic morphine-6-glucuronide following physiologic concentration of morphine in human brain. J Toxicol Sci 28:395–401. https://doi.org/10.2131/jts.28.395
37. McQuay H, Moore R (1997) Opioid problems, and morphine metabolism and excretion. The Pharmacology of Pain. Springer, New York, pp 335–360
38. NIH National Cancer Institute (2018) Naloxone (Code C62054). In: NCI Thesaurus. https://ncit.nci.nih.gov/ncitbrowser/ConceptReport.jsp?dictionary=NCI_Thesaurus&ns=NCI_Thesaurus&code=C62054
39. NIH US National Library of Medicine (2016) Naloxone. In: TOXNET. https://toxnet.nlm.nih.gov/cgi-bin/sis/search/a?dbs+hsdb:@term+@DOCNO+3279
40. Drugbank (2018) Naloxone. In: Drugbank. https://www.drugbank.ca/drugs/DB01183
41. Mistry M, Houston JB (1987) Glucuronidation in vitro and in vivo. Comparison of intestinal and hepatic conjugation of morphine, naloxone, and buprenorphine. Drug Metab Dispos Biol Fate Chem 15:710–717
42. Van Dorp E, Yassen A, Sarton E, Romberg R, Olofsen E, Danhof M, Dahan A (2006) Naloxone reversal of buprenorphine-induced respiratory depression. Anesthesiol J Am Soc Anesthesiol 105:51–57
43. Olofsen E, van Dorp E, Teppema L, Aarts L, Smith TW, Dahan A, Sarton E (2010) Naloxone reversal of morphine- and morphine-6-glucuronide-induced respiratory depression in healthy volunteers—a mechanism-based pharmacokinetic–pharmacodynamic modeling study. Anesthesiol J Am Soc Anesthesiol 112:1417–1427. https://doi.org/10.1097/ALN.0b013e3181d5e29d
44. Cassel JA, Daubert JD, DeHaven RN (2005) [3H]Alvimopan binding to the μ opioid receptor: comparative binding kinetics of opioid antagonists. Eur J Pharmacol 520:29–36. https://doi.org/10.1016/j.ejphar.2005.08.008
45. Wilkerson P, Zhou X, Przekwas A, Buhrman J, Cheng H (2009) Virtual body generator for anthropometry and physiology based modeling. SAE Technical Paper. https://www.sae.org/publications/technical-papers/content/2009-01-2280/
46. Wilkerson P, Pzrekwas A (2007) Integrated modeling framework for anthropometry and physiology virtual body. CFD Research Corp, Huntsville AL. https://apps.dtic.mil/dtic/tr/fulltext/u2/a472630.pdf
47. Müller LO, Toro EF (2014) Enhanced global mathematical model for studying cerebral venous blood flow. J Biomech 47:3361–3372. https://doi.org/10.1016/j.jbiomech.2014.08.005
48. Lötsch J, Skarke C, Schmidt H, Liefhold J, Geisslinger G (2002) Pharmacokinetic modeling to predict morphine and morphine-6-glucuronide plasma concentrations in healthy young volunteers. Clin Pharmacol Ther 72:151–162. https://doi.org/10.1067/mcp.2002.126172
49. Dershwitz M, Walsh JL, Morishige RJ, Connors PM, Rubsamen RM, Shafer SL, Rosow CE (2000) Pharmacokinetics and pharmacodynamics of inhaled versus intravenous morphine in healthy volunteers. Anesthesiol J Am Soc Anesthesiol 93:619–628
50. Bouw R, Ederoth P, Lundberg J, Ungerstedt U, Nordström CH, Hammarlund-Udenaes M (2001) Increased blood–brain barrier permeability of morphine in a patient with severe brain lesions as determined by microdialysis. Acta Anaesthesiol Scand 45:390–392. https://doi.org/10.1034/j.1399-6576.2001.045003390.x
51. Fryar CD, Kruszan-Moran D, Gu Q, Ogden CL (2018) Mean body weight, weight, waist circumference, and body mass index among adults: United States, 1999–2000 through 2015–2016. https://www.cdc.gov/nchs/data/nhsr/nhsr122-508.pdf
52. Ederoth P, Tunblad K, Bouw R, Johan C, Lundberg F, Ungerstedt U, Nordström CH, Hammarlund-Udenaes M (2004) Blood–brain barrier transport of morphine in patients with severe brain trauma. Br J Clin Pharmacol 57:427–435. https://doi.org/10.1046/j.1365-2125.2003.02032.x
53. Aitkenhead AR, Derbyshire DR, Pinnock CA, Achola K, Smith G (1984) Pharmacokinetics of intravenous naloxone in healthy volunteers. Anesthesiol J Am Soc Anesthesiol 61:A381–A381
54. McDonald R, Lorch U, Woodward J, Bosse B, Dooner H, Mundin G, Smith K, Strang J (2017) Pharmacokinetics of concentrated naloxone nasal spray for opioid overdose reversal: Phase I healthy volunteer study. Addiction 113:484–493. https://doi.org/10.1111/add.14033
55. Unbound Medicine (2018) morphine | Davis's Drug Guide. https://www.drugguide.com/ddo/view/Davis-Drug-Guide/51518/all/morphine
56. Carleton BC, Cipolle RJ, Larson SD, Canafax DM (1991) Method for evaluating drip-rate accuracy of intravenous flow-regulating devices. Am J Hosp Pharm 48:2422–2426. https://doi.org/10.1093/ajhp/48.11.2422
57. Rooker JC, Gorard DA (2007) Errors of intravenous fluid infusion rates in medical inpatients. Clin Med Lond Engl 7:482–485. https://doi.org/10.7861/clinmedicine.7-5-482
58. Hoare SRJ, Pierre N, Moya AG, Larson B (2018) Kinetic operational models of agonism for G-protein-coupled receptors. J Theor Biol 446:168–204. https://doi.org/10.1016/j.jtbi.2018.02.014
59. Lane JR, May LT, Parton RG, Sexton PM, Christopoulos A (2017) A kinetic view of GPCR allostery and biased agonism. Nat Chem Biol 13:929–937. https://doi.org/10.1038/nchembio.2431
60. Strasser A, Wittmann H-J, Seifert R (2017) Binding kinetics and pathways of ligands to GPCRs. Trends Pharmacol Sci 38:717–732. https://doi.org/10.1016/j.tips.2017.05.005
61. Ben-Tal A, Smith JC (2008) A model for control of breathing in mammals: coupling neural dynamics to peripheral gas exchange and transport. J Theor Biol 251:480–497. https://doi.org/10.1016/j.jtbi.2007.12.018
62. Ursino M, Magosso E, Avanzolini G (2001) An integrated model of the human ventilatory control system: the response to hypercapnia. Clin Physiol Oxf Engl 21:447–464. https://doi.org/10.1046/j.1365-2281.2001.00349.x
63. Boyer EW (2012) Management of opioid analgesic overdose. N Engl J Med 367:146–155. https://doi.org/10.1056/NEJMra1202561
64. Loimer N, Schmid R, Grünberger J, Linzmayer L (1990) Naloxone induces miosis in normal subjects. Psychopharmacology 101:282–283. https://doi.org/10.1007/BF02244141
65. Zakaria Z, Badhan R (2018) Development of a region-specific physiologically based pharmacokinetic brain model to assess hippocampus and frontal cortex pharmacokinetics. Pharmaceutics 10:14. https://doi.org/10.3390/pharmaceutics10010014
66. Jamei M, Bajot F, Neuhoff S, Barter Z, Yang J, Rostami-Hodjegan A, Rowland-Yeo K (2014) A mechanistic framework for in vitro–in vivo extrapolation of liver membrane transporters: prediction of drug–drug interaction between rosuvastatin and cyclosporine. Clin Pharmacokinet 53:73–87. https://doi.org/10.1007/s40262-013-0097-y

67. Fishman RA (1992) Cerebrospinal fluid in diseases of the nervous system. WB Saunders company, Philadelphia
68. Reiber H (2003) Proteins in cerebrospinal fluid and blood: barriers, CSF flow rate and source-related dynamics. Restor Neurol Neurosci 21:79–96
69. Orešković D, Klarica M (2010) The formation of cerebrospinal fluid: nearly a hundred years of interpretations and misinterpretations. Brain Res Rev 64:241–262. https://doi.org/10.1016/j.brainresrev.2010.04.006
70. May C, Kaye J, Atack JR, Schapiro MB, Friedland RP, Rapoport SI (1990) Cerebrospinal fluid production is reduced in healthy aging. Neurology 40:500–500. https://doi.org/10.1212/wnl.40.3_part_1.500
71. Kroin JS, Ali A, York M, Penn RD (1993) The distribution of medication along the spinal canal after chronic intrathecal administration. Neurosurgery 33:226–230. https://doi.org/10.1227/00006123-199308000-00007
72. Edsbagge M, Tisell M, Jacobsson L, Wikkelso C (2004) Spinal CSF absorption in healthy individuals. Am J Physiol-Regul Integr Comp Physiol 287:R1450–R1455. https://doi.org/10.1152/ajpregu.00215.2004
73. Veening JG, Barendregt HP (2010) The regulation of brain states by neuroactive substances distributed via the cerebrospinal fluid: a review. Cerebrospinal Fluid Res 7:1. https://doi.org/10.1186/1743-8454-7-1
74. Wong AD, Ye M, Levy AF, Rothstein JD, Bergles DE, Searson PC (2013) The blood-brain barrier: an engineering perspective. Front Neuroeng 6:7. https://doi.org/10.3389/fneng.2013.00007
75. McNamara PJ, Leggas M (2009) Chapter 7—drug distribution. In: Hacker M, Messer W, Bachmann K (eds) Pharmacology. Academic Press, San Diego, pp 113–129
76. Morrish GA, Foster DJR, Somogyi AA (2006) Differential in vitro inhibition of M3G and M6G formation from morphine by (R)- and (S)-methadone and structurally related opioids. Br J Clin Pharmacol 61:326–335. https://doi.org/10.1111/j.1365-2125.2005.02573.x